The UW Hand: A Low-cost, 20-DOF Tendon-driven Hand with Fast and Compliant Actuation

Zhe Xu · Vikash Kumar · Emanuel Todorov

Abstract We describe the process of designing and building a 20 degrees-of-freedom tendon-driven anthropomorphic robotic hand. We use 3D printing technology to reduce cost and save time. The entire mechanism is easily assembled thanks to our Snap-On joint design. The fingers are modular and can be individually modified with little effort. The hand is actuated by new pneumatic system consisting of an assembly of 40 low-friction cylinders, and fast proportional valves mounted off-board. The new hand described here is a drop-in replacement for the ShadowHand robot which motivated the development of the actuation system. We also use our physics engine MuJoCo to construct a detailed kinematic model of the new hand.

1 Introduction

The benefits of investigating anthropomorphic robotic hands have been widely acknowledged, and some of them have been effectively demonstrated, such as the highly biomimetic robotic hand designed for understanding the human hand (Deshpande et al, 2011), lightweight prosthetic hands with improved functionality (Touch Bionics Inc., 2009; Kyberd et al, 2001), and many other anthropomorphic robotic hands developed for investigating dexterous manipulation (Rothling et al, 2007; Grebenstein et al, 2010; Bundhoo and Park, 2005; Carrozza et al, 2006; Lovchik and Diftler, 1999; Lotti et al, 2005; Yamano and Maeno, 2005; Mouri et al, 2002; Ueda et al, 2005; Demers and Gosselin, 2011).

Zhe Xu · Vikash Kumar · Emanuel Todorov
University of Washington, Seattle, WA, USA
E-mail: zhexu@cs.washington.edu,
vikash@cs.washington.edu, todorov@cs.washington.edu

Fig. 1: The 3D-printed 20-DOF anthropomorphic robotic hand.

However, it is also widely accepted that the cost and time needed to develop a research-oriented, custom-designed anthropomorphic robotic hand is often prohibitive. The performance of a robotic hand can be affected by many factors, such as the finger length, the range of motion (ROM) of the joints, the weight of the robotic hand, or transmission types. Many researches had to shape their control goals by the limits of commercially available anthropomorphic robotic hands due to the fact that even the slightest modification on those off-the-shelf robotic hands could easily result in months of waiting.

For those researches focusing on the hardware aspects of anthropomorphic robotic hands, it is also challenging to modify the design or improve the function-

ality of an existing system in a short period of time. This is because each of the design iterations needs to go through the validation of physical tests before any useful information can be collected for planning any improvement. Therefore simulation as a promising tool to help evaluating the performance of robotic hands has been adopted to speed up the design process (Miller and Allen, 2004).

Many anthropomorphic robotic hands were designed to be cable-driven (Rothling et al, 2007; Grebenstein et al, 2010; Bundhoo and Park, 2005; Carrozza et al, 2006; Lovchik and Diftler, 1999; Lotti et al, 2005; Yamano and Maeno, 2005; Xu et al, 2012). On the one hand, it is intuitive to mimic the muscle-tendon mechanism of the human hand with cables and wires; on the other hand, this is because the cable-driven robotic hand system possesses several advantages including backdrivable, backlash-free, light weight, and the flexibility for the robotic hand to choose between being fully actuated and being under-actuated depending on needs of different application. So far numerous efforts have been put into the development of simulation software, however, none of the existing physics engines could handle the level of the complexities posed by a 20 degrees of freedom (DOFs), cable-driven anthropomorphic robotic hand.

In this paper, we take an alternative approach to the question of how the anthropomorphic robotic hand can be designed such that the fabrication of the robotic hand is fast, the cost of the modification and maintenance is cheap, and the control of the robotic hand is feasible by presenting the design, acutation, and modeling of the UW Hand (as shown in Figure 1) which possesses 20-DOF. Our proposed method combines adaptive design, rapid prototyping, and modeling with our physics engine called MuJoCo (Todorov et al, 2012). The resulting UW hand is composed of 31 parts in comparison to other existing robotic hands using hundreds of parts, and can be 3D-printed in 20 hours and fully assembled in 4 hours. Its size, DOFs, ROM, and actuation type can all be adjusted/changed with little effort or modification.

In the following sections, the innovative design methods of the UW hand are detailed, the pneumatic actuation system is described, and then the modeling of the robotic hand system is established to demonstrate how MuJoCo could help to speed up the control. At the end a fully assembled robotic hand system is prepared for our future work.
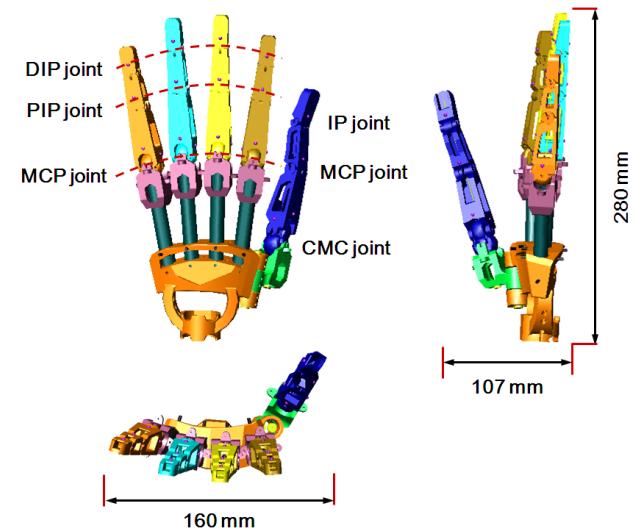
Fig. 2: 3D model of the UW hand.

2 Development of the UW hand

Although the anatomy of the human hand provides detailed sources of static models, such as joint structure, tendons routing, and layered skin, how to organically incorporate state-of-the-art engineering advances into a fully functional robotic hand system is what we want to achieve in this paper. This section describes the mechanical design and prototyping process of the UW hand.

As shown in Figure 2, Our proposed robotic hand is composed of four articulated fingers and one opposable thumb. In order to accurately match the size and shape of the human hand, a laser-scan model of a human left hand (Stratasys Corp., Eden Prairie, MN) was used to decide the length of each finger and the location of joints' axes.

There are three joints in each finger of the human hand: namely, the metacarpophalangeal (MCP), proximal interphalangeal (PIP), and distal interphalangeal (DIP). Each DIP and PIP joint possesses one DOF. The MCP joint has two DOFs: one to achieve flexion-extension and another to realize abduction-adduction finger motion. The three joints of the thumb are the carpometacarpal (CMC), metacarpophalangeal (MCP), and interphalangeal (IP) joints. Its IP and MCP joint were designed to possess one rotation DOF in the flexion-extension direction. In contrast with other fingers MCP joints, the CMC joint of the thumb has two DOFs with two non-intersecting, orthogonal axes. Table 1 lists the ROM of the UW hand.

Table 1: The joint motion limits of the anthropomorphic robotic hand

Finger	Joint	Minimum	Maximum
Index,	MCP	20° extension	90° flexion
Middle,		30° abduction	30° adduction
Ring,	PIP	0° extension	90° flexion
& Little	DIP	0° extension	90° flexion
Thumb	CMC	40° extension	90° flexion
		40° abduction	40° adduction
	MCP	0° extension	80° flexion
	IP	20° extension	90° flexion
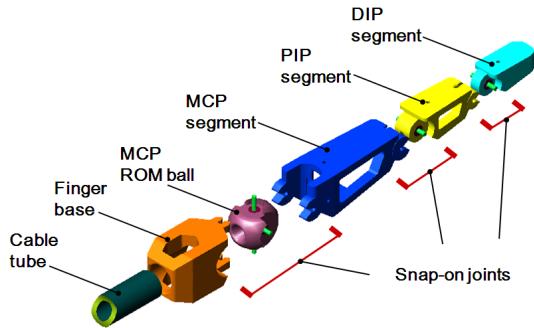
Fig. 3: Components of each finger unit.

2.1 3D-printed Lego-style, modular finger design

As previously mentioned, one of the major barriers that prevents researchers from adding modification to any existing anthropomorphic robotic hands is that the cost of time and budget. However this cost can be side stepped through the innovation of rapid prototyping technologies. As shown in Figure 3, each segment of a finger is 3D printed by the Dimension BST 768 (Stratasys Corp., Eden Prairie, MN). The resolution of the 3D printed parts is 0.025mm, and it takes only one hour to print all the components of an entire finger. Additionally the strength of the ABS plastic is sufficient to resist the induced stress of cables.

One of the important factors we believe that makes LEGO toy popular is because it allows players to inspiringly prototype their design ideas via a number of interlocking plastic bricks within a short period time. Following the same principle, our proposed robotic hand was designed to be modular and adaptable. The joint connection between two finger segments was formed by one LEGO-style Snap-On joint. As shown in Figure 3, there are three Snap-On joints in one finger. The interlocking mechanism of the Snap-On joint is composed of a 3D printed C-shaped clip on one side of the joint

Fig. 4: Two examples of assembling a Snap-On joint. *Top row: assembling a DIP hinge joint.* Bottom row: *assembling a MCP ROM-ball on to the finger base*

and a steel shaft passing through the center of the other side of the joint. After snapping into the clip, the steel shaft can be secured by the friction engagement, and a Snap-On joint is thus formed (as shown in Figure 4).

The ROM of a joint is limited by the mechanical constraints between adjacent finger segments in extreme postures and can be modified in CAD model without affecting other sites of the part. For instance, by snapping on a new MCP ROM-ball with different set of mechanical constraints, the ROM of abduction/adduction can vary from ±20 degrees to ±40 degrees easily.

In addition to simplifying the robotic hand design, the Snap-On mechanism can also help to ease the burden on assembly: by replacing a set of finger segments with shorter ones, a smaller hand will be reformed in minutes.

2.2 Adaptable cable routing

The cable routing plays an important role in control of anthropomorphic robotic hands. As shown Figure 5(a), the UW hand used four pairs of antagonistic cables to control each of its 4-DOF fingers. FEP-Coated Stainless Steel cables were chosen (0.66mm in diameter, McMaster, CA) because of its strength (178N breaking strength), high stiffness, flexibility, and its ability to slide smoothly through the cable tube.

Compared to other types of transmission, such as linkages, gears, and belts, choosing cable-driven system enables the anthropomorphic robotic hand to quickly switch between being fully actuated and being underactuated with little modification as shown in Figure 5. This in return broadens the application of the anthropomorphic robotic hand ranging from dexterous manipulation research to practical prosthetics.

Although changing the cable routing is a good way to explore the potentials of an anthropomorphic robotic hand, it is also the most time-consuming process during the assembly (e.g., 90% of the total time in our case).

(a)

(b)
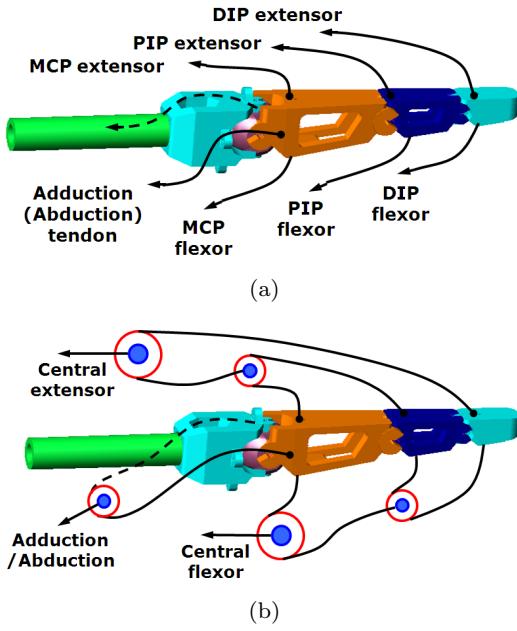
Fig. 5: Schematic drawing of two possible cable routing types. *(a)* A 4-DOF finger with four pairs of antagonistic cables (*Note:* cables originated from the DIP and PIP finger segments were passing through the center of the cable tubes in the real robotic hand, for better illustration, their routings are drawn explicitly). *(b)* A 3-DOF under-actuated finger with pulley systems.

How to efficiently optimize the cable routing and paths so that each of the finger joints can be controlled properly plays an important role in our proposed robotic hand design.

Before rushing to prototype/modify the robotic hand, the physics engine MuJoCo provided us an unique platform to evaluate our design ideas. For instance, the STL files generated for 3D printing can be directly loaded into the MuJoCo for different simulation. More details will be discussed in section 4.

3 Actuation system

The unique capabilities of the human hand have long inspired researchers in their pursuit to develop manipulators with similar "dexterity". We use this term here to refer to a combination of features: many independently-controlled DOFs, speed, strength and compliance. Simple and isolated tasks such as grasping can of course be accomplished by simpler devices. Nevertheless if robots are to perform a wider range of tasks in less structured environments than what is currently possible, they are likely to need manipulators approaching human levels of dexterity. The requirement for high dexterity natu-

rally leads to the choice of pneumatic actuation. Indeed this may be the only available technology that combines speed, strength and compliance on the mechanism level with small and lightweight actuators.
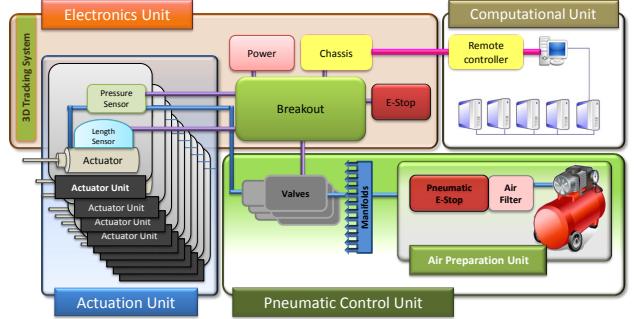
Fig. 6: Schematic drawing of the actuation system.

The actuation system used here was designed as a replacement for the built-in actuation in the Shadow-Hand robot (which we acquired recently). This new system is described in detail in a conference paper under review. The UW hand has the same mounting mechanism as the ShadowHand and the same number of tendons, so that it can be used as a drop-in replacement. Below we provide a self-contained summary of this actuation system; see Figure 6. It consists of a cylinder assembly (the actuation unit) and a rack of off-board valves (the pneumatic control unit) as well as the necessary electronics and software we have developed.

3.1 Actuation unit

The actuation unit (see Figure 7) consists of double-acting Airpel series cylinders (Airpot Corp., CT). They have stroke length of 37.5mm, can produce up to 42N of force at 90 PSI and weigh 45.7grams. Here these cylinders are used in single-acting mode: they only pull. In tendon driven systems, it is preferable to have a small force on the actuators to avoid tendon slack. We adjusted the pressure level in the "off" phase to achieve this effect while adding minimal co-activation. Figure 8 shows the entire housing assembly with the actuator units.

The UW Hand routes finger tendons via the center of the wrist joint in order to minimize the moment arms of finger tendons on the wrist joint. As a result, all finger tendons come out of the hand via an opening at the wrist. To reduce off-axis actuator loads, it is desirable to mount the cylinders so that they all point to this opening – suggesting a concave mounting plate. The back plate is free of cables and connectors and has mounting

Fig. 7: Cylinder unit (AC: Actuator, LS: Length Sensor, PS: Pressure Sensor)

holes for attachment to a robot arm. Figure: 8(d) shows the complete Muscle actuation unit without the back plate. Note that if we did not attach a length sensor to each cylinder (which doubles the cylinder diameter) the diameter of the assembly could be reduced roughly by half. This potential modification can be considered for those robotic hands whose joints are implemented with joint sensors.
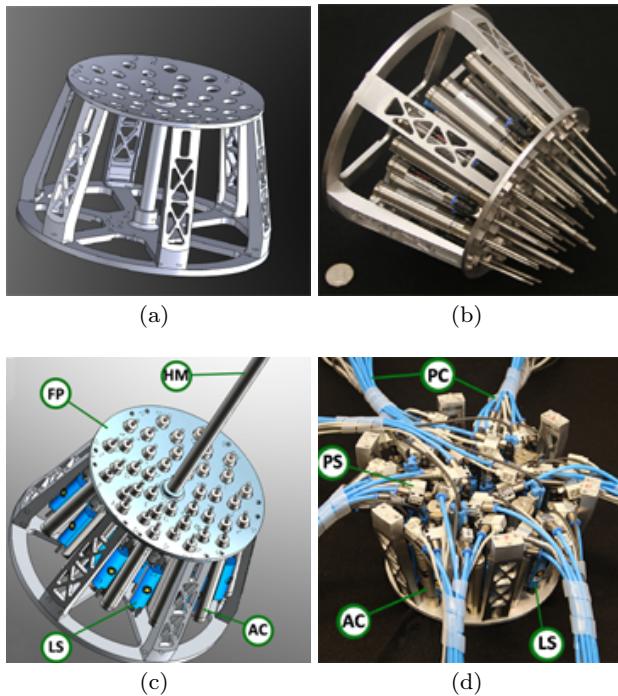
Fig. 8: Housing assembly *(a)* CAD model of the bracket; *(b)* Cylinders pointing to the wrist opening; *(c)* Housing assembly in CAD model; *(d)* Final assembly (without back plate). (FP: Front Plate, HM: Hand Mount, LS: Length Sensor, AC: Actuator, PS: Pressure Sensor)

The housing assembly weighs 660grams, and can sustain about 75N from each actuator with a safety factor of 3. When attached to a robot arm, most of this mass is near the base (elbow).

3.2 Pneumatic control unit

The pneumatic control unit shown in Figure 9 consists of forty MPYE 3/5 proportional valves from FESTO and its pneumatic peripherals such as an air compressor and air supply manifolds. The selected valves support a high flow rate of 100L/min at 90 PSI, and have bandwidth of 125Hz.

We decided to use high-end off-board valves after working with the ShadowHand robot which uses small valves mounted on-board. Such valves have insufficient flow rate – resulting in sluggishness that matches the reputation pneumatic systems have in robotics. Apart from the higher price of the valves we selected, our design has the potential disadvantage that the longer air tubes can introduce delays. However this was not the case. For the combination of tube lengths, flow rates, pressures and cylinder volumes used here, we were able to achieve maximum force in the cylinder around 10 msec after sending a command to the valve – which is faster than the response of human hand muscles to neural input.
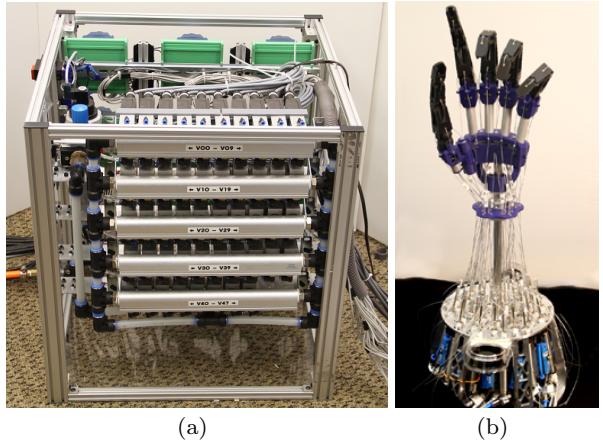
Fig. 9: The actuation system of the UW Hand. *Left:* the pneumatic control unit. *Right:* Fully assembled UW Hand.

4 MuJoCo model of the UW Hand

The variable moment arms of the UW hand closely mimic its human counter-part, and provide us an unique opportunity to investigate dexterous manipulations tasks. However, it also poses a series of challenges to the robotic hand control. Together with the information of the tendon excursion, knowing accurate moment arms at each
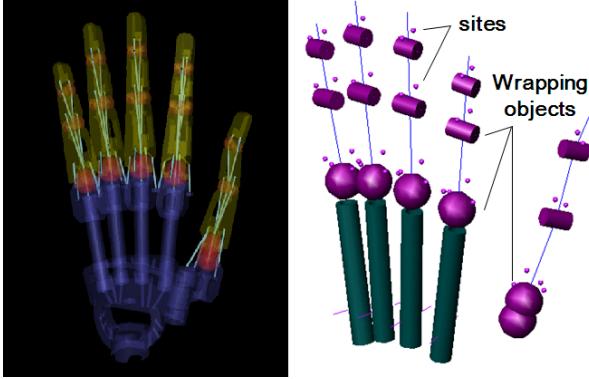
Fig. 10: MuJoCo model of the UW hand. *Left:* kinematic model of the robotic hand visualized in OpenGL. *Right:* The model of the cable paths.

joint of the finger can allow us to easily compute the kinematic configuration for the corresponding finger.

Instead of complicating the mechanical structure of the UW hand by adding multiple joint sensors, we constructed a kinematic model of the UW hand and its cable paths (as shown in Figure 10). This was done by taking the numeric data from the CAD file used to 3D-print the robotic hand, and importing it in an XML file that is then read by our modeling software. Our software – called MuJoCo which stands for Multi-Joint dynamics with Contact – is a full-featured new physics engine, with a number of unique capabilities including simulation of cable actuation via complex surfaces. In this paper we only use the kinematic modeling features of the engine, as well as the built-in OpenGL visualization.
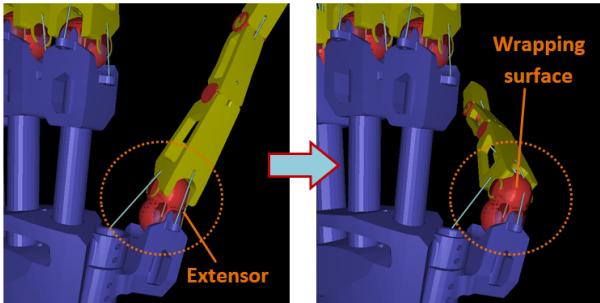
Fig. 11: The thumb Extensor wrapping at the CMC joint during the flexion motion.

The skeletal modeling approach is standard: the system configuration is expressed in joint space, and forward kinematics are used at each time step to compute the global positions and orientations of the body segments along with any objects attached to them. Cable

modeling is less common and so we describe our approach in more detail. The path of the cable is determined by a sequence of routing points (or sites) as well as geometric wrapping objects which can be spheres or cylinders (as shown in Figure 10). As shown in Figure 11 the software computes the shortest path that passes through all sites defined for a given, and does not penetrate any of the wrapping objects (i.e. the path wraps smoothly over the curved surfaces). The latter computation is based on the Obstacle Set method previously developed in biomechanics.

Let $\mathbf{q}$ denote the vector of joint angles, and $\mathbf{s}_1(\mathbf{q}), \cdots, \mathbf{s}_N(\mathbf{q})$ denote the 3D positions (in global coordinates) of the routing points for a given cable. These positions are computed using forward kinematics at each time step. Then the cable length is

$$L(\mathbf{q}) = \sum_{n=1}^{N-1} \left((\mathbf{s}_{n+1}(\mathbf{q}) - \mathbf{s}_n(\mathbf{q}))^T (\mathbf{s}_{n+1}(\mathbf{q}) - \mathbf{s}_n(\mathbf{q})) \right)^{1/2}$$

The terms being summed are just the Euclidean vector norms $\|\mathbf{s}_{n+1} - \mathbf{s}_n\|$, however we have written them explicitly to clarify the derivation of moment arms below. When the cable path encounters a wrapping object, additional sites are dynamically created at points where the cable path is tangent to the wrapping surface. These sites are also taken into account in the computation of lengths and moment arms.

Moment arms are often defined using geometric intuitions – which work in simple cases but are difficult to implement in general-purpose software that must handle arbitrary spatial arrangements. Instead we use the more general mathematical definition of moment arm, which is the gradient of the cable length with respect to the joint angles. Using the chain rule, the vector of moment arms for our cable is

$$\frac{\partial L(\mathbf{q})}{\partial \mathbf{q}} = \sum_{n=1}^{N-1} \left(\frac{\partial \mathbf{s}_{n+1}(\mathbf{q})}{\partial \mathbf{q}} - \frac{\partial \mathbf{s}_n(\mathbf{q})}{\partial \mathbf{q}} \right)^T \frac{\mathbf{s}_{n+1}(\mathbf{q}) - \mathbf{s}_n(\mathbf{q})}{\|\mathbf{s}_{n+1}(\mathbf{q}) - \mathbf{s}_n(\mathbf{q})\|}$$

This expression can be evaluated once the site Jacobians $\partial \mathbf{s}/\partial \mathbf{q}$ are known. Our software automatically computes all Jacobians, and so the computation of moment arms involves very little overhead.

Numerical values for the moment arms change with hand configuration in a complex way, and are automatically recomputed at each time step. Moment arms are useful for computing the cable velocities given the joint velocities:

$$\dot{L} = \frac{\partial L(\mathbf{q})}{\partial \mathbf{q}} \dot{\mathbf{q}}$$

and also for computing the vector of joint torques τ caused by scalar tension f applied to the cable by the corresponding linear actuator:

$$\tau = \left(\frac{\partial L(\mathbf{q})}{\partial \mathbf{q}} \right)^T f$$

Note that these are the same mappings as the familiar mappings between joint space and end-effector space, except that the Jacobian $\partial L/\partial \mathbf{q}$ here is computed differently. Another difference of course is that cables can only pull, so $f \leq 0$.

Examples of measured moment arms of the UW hand's index finger are shown in Figure 12.

(a) DIP joint   (b) PIP joint

(c) MCP flexion joint   (d) MCP abduction/adduction joint
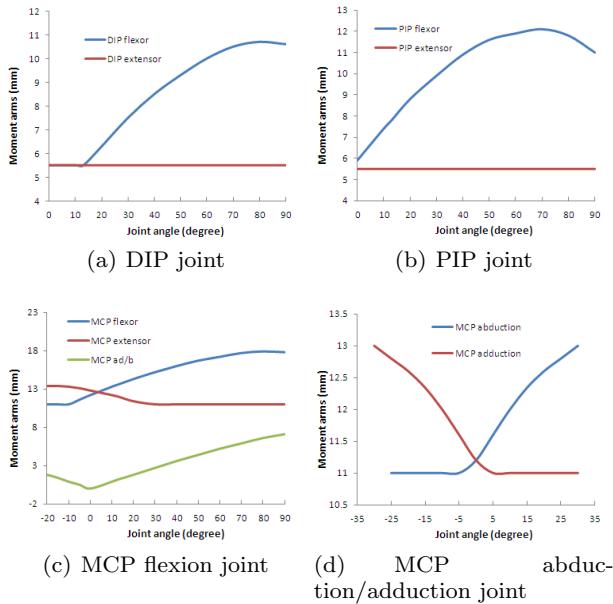
Fig. 12: Moment arms at different joints of the index finger of the robotic hand. *(a)* Moment arms at the DIP joint. *(b)* Moment arms at the PIP joint. *(c)* Moment arms at the MCP flexion joint. *(d)* Moment arms at the MCP abduction/adduction joint.(*Note:* Flexion and abduction motions have positive angles, flexion; extension and adduction motions have negative angles.)

5 Preliminary results

As shown in Figure 13, the UW hand was fully assembled and tested by using our proposed pneumatic actuation system.[1] Note that there were no joints sensors or complicated control algorithms were implemented to the system at this stage. The compliance of the pneumatic actuation system allowed us to manually pause the movement of the UW hand without causing any damages to the robotic hardware or the person's hand.

---

[1] The multimedia extension page is found at `http://homes.cs.washington.edu/~vikash/Projects/IJRR.mp4`
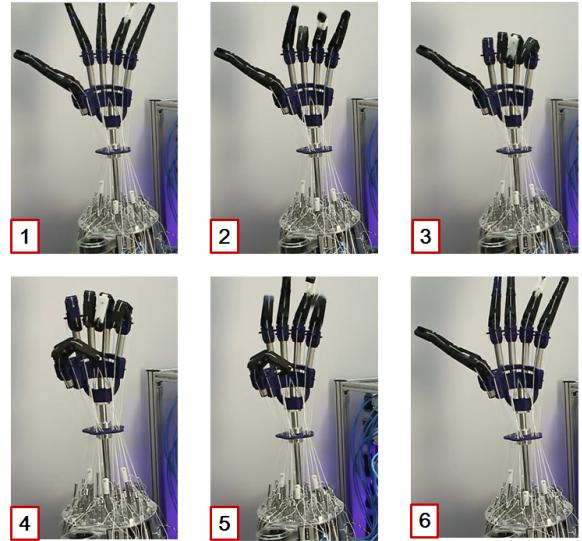
Fig. 13: The sequence of images of the UW hand performing envelop grasp.

6 Conclusion and future work

We have described the method of designing and modeling a 20-DOF anthropomorphic robotic hand. Our proposed robotic hand has 31 components, and can be manufactured in 24 hours. Important parameters such as finger length, DOF, and ROM of the robotic hand can all be individually changed with little effort or modification. For evaluating design ideas and speeding up our design cycle, we used MuJoCo to develop the kinematic model of the hand. Our proposed design has the potential to become an important tool for assisting robotic hand researchers to efficiently investigate different control methods.

In future work we plan to integrate tactile sensors for the UW hand, as well as develop suitable control strategies that enable dexterous manipulation.

References

Bundhoo V, Park E (2005) Design of an artificial muscle actuated finger towards biomimetic prosthetic hands. In: 12th International Conference on Advanced Robotics, 2005. ICAR '05. Proceedings.,, pp 368 –375

Carrozza MC, Cappiello G, Micera S, Edin BB, Beccai L, Cipriani C (2006) Design of a cybernetic hand for perception and action. Biol Cybern 95(6):629–644

Demers LAA, Gosselin C (2011) Kinematic design of a planar and spherical mechanism for the abduction of the fingers of an anthropomorphic robotic hand.

In: 2011 IEEE International Conference on Robotics and Automation (ICRA),, pp 5350 –5356

Deshpande AD, Xu Z, Weghe MJV, Brown BH, Ko J, Chang LY, Wilkinson DD, Bidic SM, Matsuoka Y (2011) Mechanisms of the Anatomically Correct Testbed Hand. IEEE/ASME Transactions on Mechatronics (99):1–13

Grebenstein M, Chalon M, Hirzinger G, Siegwart R (2010) Antagonistically driven finger design for the anthropomorphic DLR Hand Arm System. In: 2010 10th IEEE-RAS International Conference on Humanoid Robots (Humanoids),, pp 609 –616

Kyberd PJ, Light C, Chappell PH, Nightingale JM, Whatley D, Evans M (2001) The design of anthropomorphic prosthetic hands: A study of the southampton hand. Robotica 19(6):593–600

Lotti F, Tiezzi P, Vassura G, Biagiotti L, Palli G, Melchiorri C (2005) Development of UB Hand 3: Early results. In: Proceedings of the 2005 IEEE International Conference on Robotics and Automation, pp 4488–4493

Lovchik C, Diftler M (1999) The Robonaut hand: a dexterous robot hand for space. In: Proceedings of the 1999 IEEE International Conference on Robotics and Automation., vol 2, pp 907–912

Miller A, Allen P (2004) Graspit! a versatile simulator for robotic grasping. IEEE Robotics Automation Magazine 11(4):110 – 122

Mouri T, Kawasaki H, Keisuke Y, Takai J, Ito S (2002) Anthropomorphic robot hand: Gifu hand III. In: Proc. Int. Conf. ICCAS

Rothling F, Haschke R, Steil J, Ritter H (2007) Platform portable anthropomorphic grasping with the bielefeld 20-DOF Shadow and 9-DOF TUM hand. In: IEEE/RSJ International Conference on Intelligent Robots and Systems

Todorov E, Erez T, Tassa Y (2012) Mujoco: a physics engine for model-based control. In: IEEE/RSJ International Conference on Intelligent Robots and Systems

Touch Bionics Inc (2009) www.touchbionics.com

Ueda J, Ishida Y, Kondo M, Ogasawara T (2005) Development of the NAIST-Hand with vision-based tactile fingertip sensor

Xu Z, Kumar V, Matsuoka Y, Todorov E (2012) Design of an anthropomorphic robotic finger system with biomimetic artificial joints. In: 2012 4th IEEE RAS EMBS International Conference on Biomedical Robotics and Biomechatronics (BioRob), pp 568 – 574

Yamano I, Maeno T (2005) Five-fingered robot hand using ultrasonic motors and elastic elements. In: Proceedings of the 2005 IEEE International Conference on Robotics and Automation., pp 2673–2678